Available online at www.sciencedirect.com

ScienceDirect

Procedia Manufacturing 26 (2018) 228–236

Procedia MANUFACTURING

www.elsevier.com/locate/procedia

46th SME North American Manufacturing Research Conference, NAMRC 46, Texas, USA

Adaptive geometry transformation and repair for hybrid manufacturing

Maxwell Praniewicz, Thomas Kurfess, Christopher Saldana*

George W. Woodruff School of Mechanical Engineering, Georgia Institute of Technology, 801 Ferst Drive, Atlanta, Georgia 30332

* Corresponding author.
E-mail address: christopher.saldana@me.gatech.edu

Abstract

In recent years, hybrid manufacturing has transitioned from research and development to commercially available industrial machine tools. This proliferation has led to a growing interest in the unique capabilities of these machines. Manufacturers in the mold and die, oil and gas, and aerospace industries are investigating hybrid manufacturing as a means of repairing high value components to reduce operating costs. As these parts become worn or damaged and taken out of service, each has its own unique distorted and worn geometry, and requires a distinct repair plan. This requires the repair strategy for these components to adapt to these fluctuations in geometry by modifying the re-manufacturing process on a part by part basis. This paper details a method of model transformation for adaptive part repair for use in a commercial hybrid manufacturing system. Nominal CAD geometry of the component is transformed based on data captured from the actual part geometry in a two-step process. The nominal geometry is first rigidly registered to the measured part data using an iterative algorithm. Then, individual cross sections of the nominal model are then deformed to match the actual data. After this transformation, final profile geometry can be constructed by using these informed transformations. This overall hybrid repair framework is shown to be of high accuracy and capable of yielding significant improvements in material usage efficiency and processing time compared to conventional repair approaches.

Peer-review under responsibility of the scientific committee of the 4th International Conference on System-Integrated Intelligence.

Keywords: Hybrid manufacturing, part repair, adaptive repair

1. Introduction

Post processing is often required on additively manufactured (AM) components in order to bring the part to its required geometric tolerances and final surface finish. This processing often involves several steps including: heat treatment, separation from the build plate, and/or final machining. Each of these steps

2351-9789
Peer-review under responsibility of the scientific committee of the 4th International Conference on System-Integrated Intelligence.
10.1016/j.promfg.2018.07.031

requires not only additional operating time, but also transfer and set up time between processes. These setups are a large contributor to the overall cost of an AM part [1].

Hybrid manufacturing seeks to reduce some of this cost by combining additive manufacturing with traditional subtractive manufacturing. This allows the part to remain fixtured in one machine while switching between adding and subtracting material throughout the build process. Commercial hybrid manufacturing machines combine the capability of additive manufacturing to create free form geometries with little material waste with the well-established accuracy and repeatability of machining. It also allows for unique processes such as the finishing of previously inaccessible internal geometries such as cooling channels.

These systems are not only capable of manufacturing new components, but also possess the ability to repair damaged components. This potential has piqued the interest of the aerospace and mold and die industries, where repairs on worn high value items can have significant financial impact. Components previously repaired by hand or through limited automation can now be completely repaired in a single machine setup [2, 3]. While these systems have existed for some time in the research community [4, 5], only recently have large machine tool manufacturers begun to create their own hybrid machines [6]. This has greatly decreased the barrier to entry into this developing technology for large scale manufacturing companies.

One case where hybrid manufacturing has benefited the aerospace industry is the repair of compressor blades. Throughout their use, these blades experience wear at the blade tip and must be repaired. This is done by removing the worn area, welding additional material to the blade tip, then machining and blending the geometry back to correct form. These blades also experience varying degrees of warp during normal use, and while this deformation may not be significant enough to scrap the part, it dramatically increases the complexity of a repair. To accommodate this, extra material is deposited during the welding stage and a margin of weld material is left after the machining process. This extra weld material must then be blended back into the original blade material by a skilled technician. This blend is required to make a smooth transition between original blade and the newly machined surface. The final inspection of the blade is then completed on the resulting machined geometry. Significant process savings could be made if the process could be adapted to differences in individual part geometry.

In order to adapt the process to individual blades, tooth paths must be adapted on a part-by-part basis. Qi et al. describe an addaptive additive repair method for compressor blades; however, it is adaptive only in the deposition method, not the overall geometry to be repaired [7, 8]. Therefore, the geometry of a worn or welded blade must be reconstructed. Reconstruction of compressor blade geometry has been studied in Ref. [9], however this method requires a full scan of the actual blade geometry in order to be implemented. Moreover, this method uses the nominal model to repair the actual geometry instead of adapting to match the actual part. This could lead to the creation of geometries which do not transition evenly into the parent material. The approach used in Ref. [10] also requires an entire scan of the blade geometry, which requires significant process time and is not easily implementable within a commercial hybrid manufacturing machine. Other methods of airfoil reconstruction such as the one presented in Ref. [11], do not extend the geometric reconstruction to unknown blade profiles.

This paper demonstrates a modeling strategy for use in a hybrid manufacturing system to accurately reconstruct worn or unknown geometry of a generic compressor blade. In the additive phase, this strategy reconstructs the blade tip geometry in order to improve weld placement and increase material efficiency. In the subtractive phase, this algorithm reconstructs the geometry of the actual blade and creates geometry for

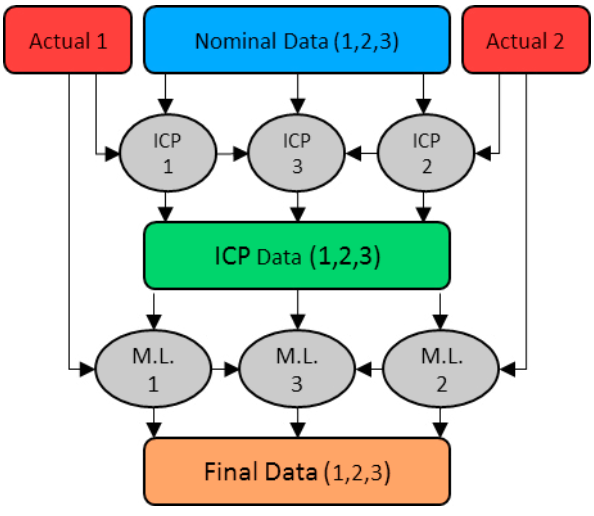

Fig. 1. Process for unknown surface modelling

the blade tip, which completes the surface to be machined. The final part qualification is then compared against the transformed geometry. The objective is not to return the actual geometry back to the nominal form, but instead to minimize deviation on the machined surface of the welded blade to eliminate expensive hand blending.

2. Methodology

The following strategy is designed to be implemented in conjunction with typical on-machine metrology technology available in hybrid manufacturing systems, namely coordinate measurement machine (CMM) type inspection probes. These devices can be used for part setup or mid cycle inspection and return the coordinates of the points probed, which can be accessed by programs in the controller or read by a networked computer. This data

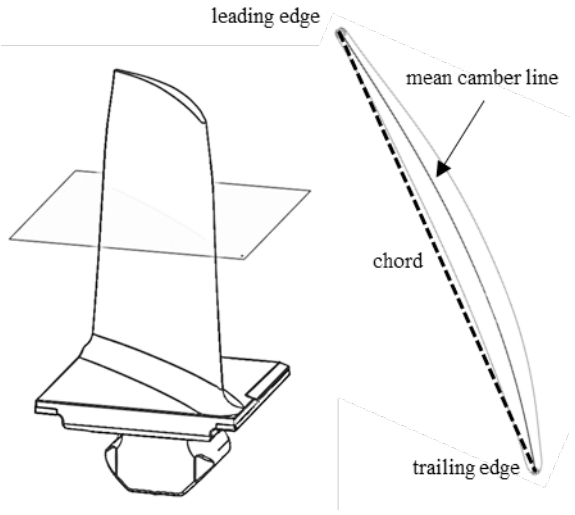

Fig.2. Image of compressor blade and cross section

can then be manipulated by software located on the computer. Commands based on this data can then be uploaded and executed by the machine tool.

Figure 1 depicts the process for the geometry manipulation. Data from the actual blade can be captured in the form of two-dimensional (2D) sections, an example of which is shown in Fig. 2. The nominal blade data can then be manipulated to match the actual data via a two-step process using a combination of rigid and non-rigid registration techniques. In this manner, transformations required to manipulate the nominal model to match known profiles of the existing geometry can be used to make informed transformations of on a third profile of the nominal model. These transformed and created profiles are then used to create a final model of the blade to be processed during the repair.

2.1. Blade geometry input

The actual blade geometry is captured by probing a number of cross sections (at least two) at prescribed heights along the radial direction of the blade below the region which is to be repaired. The following formulation makes use of two profiles for this purpose, where a greater number of profiles would increase the accuracy of the algorithm. The profile's mean camber line, shown in Fig. 2 is defined as continuous curve which lies equidistant to either side of the blade's pressure surfaces. The calculation of this mean line is well documented [12] and can be constructed using available commercial programs [13]. The blade's profile, defined as a matrix of 3D coordinates $P_z = [P_0 \dots P_m]$, a mean line, and its assigned thickness distribution can be computed where it is represented as a periodic interpolating cubic spline curve with a control point vector $Cp_z = [CP_0 \dots CP_n]$ and a knot vector $t_z = [t_0 \dots t_{n+4}]$. $N_z = [N_{0,3}(t_z) \dots N_{n,3}(t_z)]$ are the b-spline basis functions with the subscript z denoting the section height.

$$MCL_z(t_z) = \sum_{i=0}^{n} Cp_{z,i} N_{i,3}(t_z) \tag{1}$$

The thickness distribution of the blade, defined as the normal distance from the mean camber line to the blade profile, is also imported. The thickness distribution for a given profile can be defined as:

$$Td_z = f(t_z) \tag{2}$$

The nominal geometry is input in a similar manner at three profiles. Two of these profiles are evaluated at the same height as probed on the actual geometry, while the third is the profile at the tip of the blade. These are imported as Pn_z, $MCLn_z(t_z)$, $Tdn_z(t_z)$ where *n* denotes the nominal model.

2.2. Rigid profile registration

The nominal geometry must first be rigidly aligned with the actual geometry in three-dimensional (3D)

space. This operation accounts for translational or rotational offsets that may occur between the fixtured actual part and its digital nominal counterpart. Due to changes in the actual geometry caused by deformations such as blade lean or twist, the overall geometries cannot be registered and instead must be registered section by section. It is important that each nominal profile Pn_z must be considered against its counterpart P_z in the actual geometry. This will account for any distortions that would change the placement of P_i relative to the position of P_{i+1}.This is accomplished using a conventional iterative closest point (ICP) algorithm [14], which minimizes the overall mean squared distance between two point sets. This algorithm is iterated until the decrease in error between successive iterations is less than 0.1%. The required 3x3 rotation matrix R and the 3x1 translation matrix T applied to meet this result are then reported. This operation is performed for the two profiles on the actual geometry, yielding R_1, R_2, T_1, T_2.

The third profile (e.g., tip profile) of the nominal blade must then be transformed. Since there is no information known about the tip profile of the actual blade, an informed transformation must be made using the previous two transformations. A linear approximation for both R_3 and T_3 can be made based on $[R_1, R_2]$ and $[T_1, T_2]$ respectively. In order to determine R_3, R_1 and R_2 must first be decomposed into their respective angular rotations about the global axes, θ_x, θ_y, and θ_z. Ref. [15] demonstrates a method for this procedure, but its application yields two possible solutions. The correct solution can be determined by once again transforming Pn_z by the computed angles and analyzing the mean squared error between the data sets. The rotation angles for the third profile can then be calculated. The final rotation matrix can then be calculated by combining the individual X, Y, and Z rotations.

The translation T_3 can be calculated in a similar manner. The final translations and rotations can then be applied to the profiles. Since the transformation is rigid, the mean line for each curve can be transformed by manipulating the spline control points as one rigid data set. The transformed profiles, control points, and curves can then be written as:

$$PT_z = R_z Pn_z + T_z \tag{3}$$

$$CpT_z = R_z Cpn_z + T_z \tag{4}$$

$$MCLT_z(t_z) = \sum_{i=0}^{n} CpT_{z,i} N_{i,3}(t_z) \tag{5}$$

2.3. Non-rigid transformation

While the nominal profiles have been transformed to match the location and orientation of the actual profiles, deviations may still exist in the geometry of the profiles themselves. The nominal profiles must then be distorted to match the actual blade geometry. Since the mean camber line is used to define the shape of the profile, comparison between MCL_z and $MCLT_z$ can be used to calculate deviations in the profile geometry. The geometry of these curves can be compared by examining the b-spline control points. The deviation between these control points can be defined as $D_{z,i}$. The tip mean camber line must also be transformed to capture the trend of any profile deviation that occurs along the radial direction of the blade. This is done using a linear interpolation on a control point to control point basis. The final transformed control points for the b-spline curve can then be defined as:

$$Cpf_z = CpT_z + D_z \tag{6}$$

Thus, the final mean camber lines for the blade can be defined as:

$$MCLF_z(t_z) = \sum_{i=0}^{n} CpF_{z,i} N_{i,3}(t_z) \tag{7}$$

2.4. Profile creation

Once the mean camber lines have been manipulated, the final blade profiles can be created. This is completed by evaluating the thickness distribution along the length of the curve, and projecting points normal to the curve. First, the derivative $MCLF_z'$ is calculated, then vectors normal to the curve are calculated within the plane of the profile and normalized, defined as $N_z(t)$. Points are then placed on either side of $MCLF_z(t)$ at a distance $Td_z(t)$ along the normal vector $N_z(t)$. Since the thickness distribution of the actual blade is known, the nominal thickness distribution can be replaced by the actual in the first two sections. The final profiles for each

contour (e.g., i = 1,..,n) can then be evaluated in the following general form:

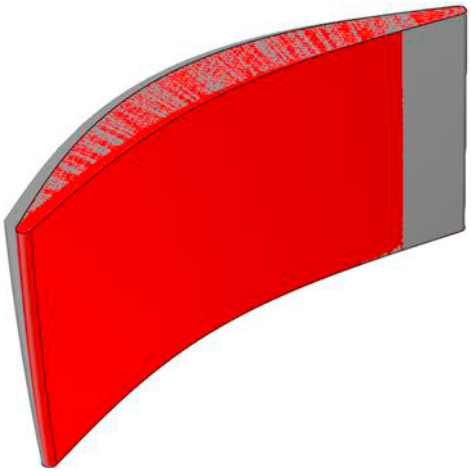

Fig 3. Overlay of the actual service part (red) and its nominal cad model (grey)

$$Pf_i = MCLF_i(t) +/- Td_i(t)N_i(t) \qquad (8)$$

The leading and trailing edge profiles can then be created by making circular arcs of radius $Td(0)$ and $Td(t_{n+4})$ at their respective ends of the profile which span between the two points placed normal to the curve in the previous step. The completed profiles can then be lofted to create a surface body or solid model.

3. Results

A nominal compressor blade was designed to determine the accuracy of the proposed hybrid repair framework. This was done by assigning a thickness distribution to a constructed profile mean line. This single section was then translated and rotated about the blades vertical axis to create two additional profiles. Cubic splines were fitted to all three profiles and lofted to create a solid model.

To create a used blade for repair, artificial defects were introduced to manipulate the nominal model. These artificial defects included adding twist to the blade and changes to the blade chord length, simulating airfoil damage that may occur in regular use. Twist was implemented by manipulating the rotations about the vertical axis, while chord length changes were implemented by manipulating the profile mean line for each section. Although not used in the transformation process, the tip section of the actual blade was constructed to serve as a visual reference and comparison tool.

To test this algorithm, a used blade segment was generated to include a twist along the radial direction of the blade. This geometry (red) is shown in comparison to the previously created nominal model (grey) in Fig. 3. Once generated, these geometries were input into the previously described algorithm. Figure 4. shows these profiles throughout various stages of the algorithm. The ICP algorithm transforms the lower two profiles rigidly to minimize the overall distance between the two profiles, but deviations between the mean camber lines of the second profile still remain. The third (tip) profile also is transformed to an appropriate position. Figure 4c shows the exact alignment of both the profile mean lines and the profiles themselves. This is expected, as the algorithm

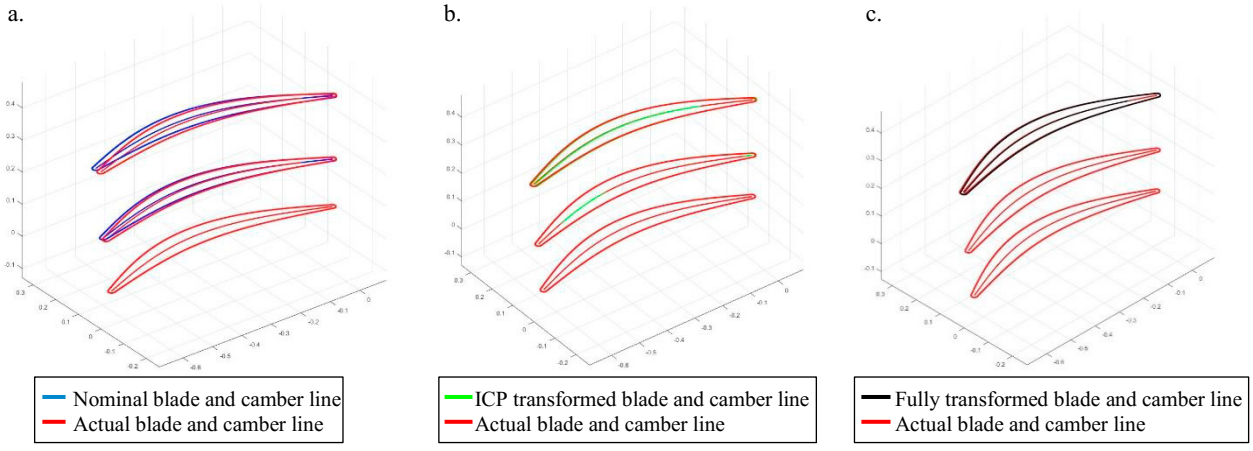

Figure 4: Evolution of nominal geometry throughout the registration process; (a) nominal geometry, (b) rigid registration, (c) profile mean line transformation

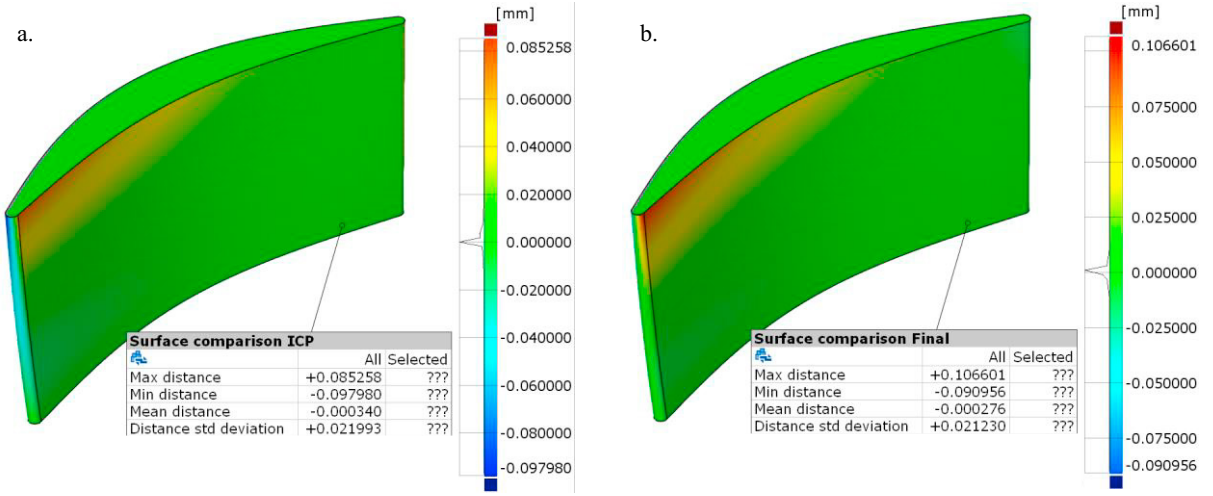

Fig. 5. Surface comparison: (a) rigidly registered blade to actual geometry (b) completely registered blade to actual geometry

should directly manipulate the nominal curve to fit the actual curves.

Figure 5a shows a surface comparison between the generated model and the actual blade after the completion of rigid registration. This shows a mean surface profile deviation over the entire blade of 0.00034 mm, with a maximum deviation of -0.098 mm occurring at the tip of the blade. There is also deviation reported along the leading edge of the blade, showing a shift in the profiles along the chordal direction of the blade that increases along the radial direction of the blade. The histogram next to the error bar shows that much of data points lie very close to no deviation and the standard deviation of the data was calculated as 0.022 mm.

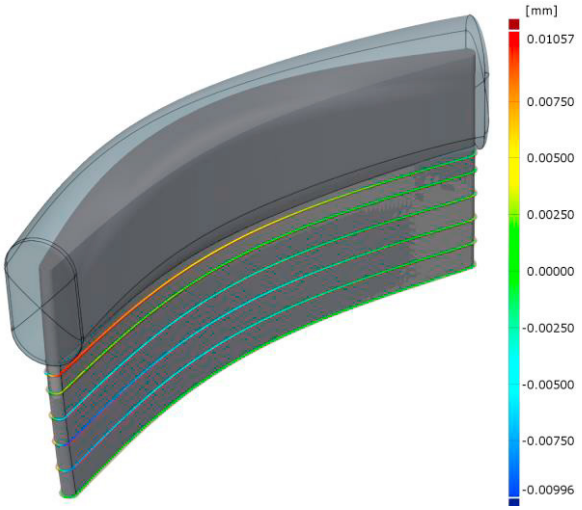

Fig 6. Profile comparison of completely registered blade (opaque) to actual welded geometry (transparent)

Figure 5b shows the final surface comparison after the completion of the algorithm. Notably, the deviations along the leading edge have greatly decreased and have localized to the region between the second and third profiles. The maximum deviation has also increased to 0.107 mm due to the interpolated transformation of the mean line.

4. Discussion

In the case of blade re-manufacturing, the third (tip) profile is unknown and must be machined from the additively deposited material. The machining strategy based on this transformed geometry must not gouge the original blade material, but also not leave excess weld material which must later be removed and blended into the original material. Therefore, it is important for the algorithm to accurately construct the region in which the welded material meets the parent blade material. To demonstrate this, two profiles of a welded geometry and their equivalent nominal geometry were input to the hybrid repair framework. Figure 6 shows the results of these simulations. The transformed blade is shown within the transparent welded geometry. The maximum deviation between these two surfaces is 0.011 mm. This is largely due to the linear interpolation between analyzed sections. If the number of probed sections were increased, a higher order interpolation could be fit, which would better predict the deviations throughout the surface. However, this would also increase the cycle time for data acquisition due to the necessity to probe increased number of sections.

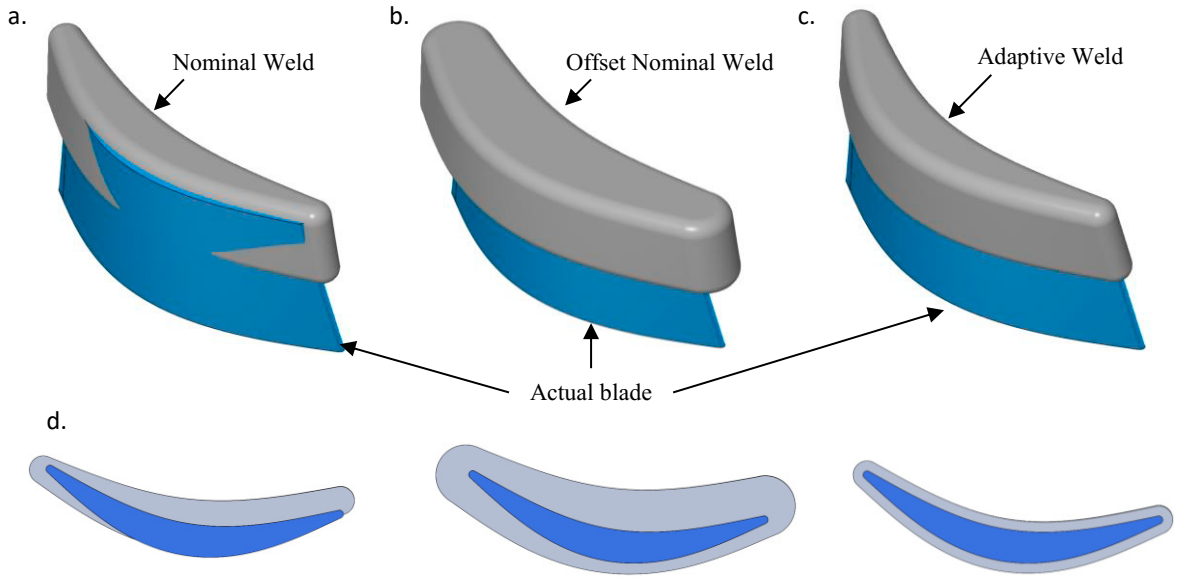

Fig. 7. Weld bead profiles superimposed on an actual geometry (a) created from the nominal data (b) created by increasing the offset of nominal weld (c) weld created using adaptive geometry. Changes in weld geometry are shown for each case at a specific cross section are shown in (d).

This adaptive geometry transformation method is also useful in the additive phase of repair. In non-adaptive hybrid repair processing, the original damaged portion of the blade is cut off from the parent material. Material is then welded to the blade along a path described by the nominal model. However, due to variations in part geometry, this nominal weld may not provide enough margin between the weld and the surface of the part to be machined for the case of a distorted blade, as shown in Fig. 7a. In practice, to accommodate for this unwanted issue, the size of the nominal weld is often increased to provide the required margin, as shown in Fig. 7b. In this manner, an adaptive hybrid repair geometry could be used to reduce wasted material and also decrease overall process time associated with machining excess additively deposited material (Fig. 7c).

Inconel 718 airfoils with varying levels of distortion were created to determine the effects of this hybrid part repair strategy, as described in Table 1.

Table 1. Parameters and performance for adaptive hybrid repair scenarios. Z represents the height above the bottom profile

		Non-Adaptive Hybrid Repair Strategy		Adaptive Hybrid Repair Strategy		Non-Adaptive vs. Adaptive Hybrid Repair Strategy		
Twist (deg/mm)	Chord Length Change (mm)	Weld Volume (mm^3)	Material Efficiency	Weld Volume (mm^3)	Material Efficiency	Increase in Machining Time (s)	Increase in Deposition Time (s)	Total Increase in Process Time
0	0	260	-	260	-	-	-	-
+0.26	0	392	66%	260	100%	+44.5	+13.0	80.1%
0	-0.125-0.02*z	385	68%	260	100%	+42.2	+12.4	75.7%
-0.26	-0.125-0.02*z	494	53%	260	100%	+79.1	+23.2	142.1%
-0.5	0	417	62%	260	100%	+52.7	+15.5	94.6%
-0.26	0	349	74%	260	100%	+29.7	+8.8	53.5%

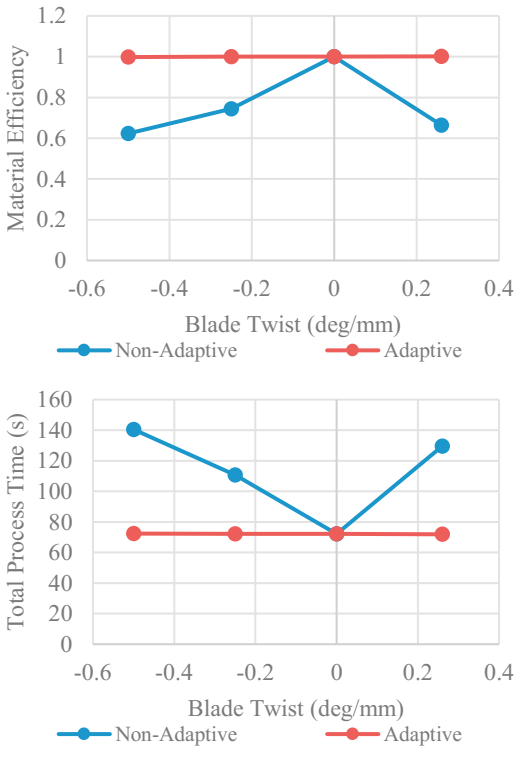

Fig. 8. (a) Material efficiency comparison between non-adaptive and adaptive strategies (b) Predicting total process time for both strategies

The adapted geometries for each of these samples were calculated. Adaptive weld geometries for each sample were created by adding a margin of 0.635 mm to the thickness distributions of each profile to allow adequate margin for tool engagement during final machining. The created surface was then clipped at a consistent height and closed to form a solid geometry. The nominal weld geometry was created using the same process. Nominal offset welds were created for each sample by increasing the thickness of the nominal weld until the minimum required margin of 0.635 mm between the weld and the surface of the part was reached.

Material efficiencies for each sample were calculated for each sample by dividing the nominal weld volume by each sample's respective weld volume. This was done for both the non-adaptive (Fig. 7b) and adaptive (Fig. 7c) procedures. Table 1 shows the results for all 5 samples, while Fig. 8a presents the effect on material efficiency as blade distortion changes. In the non-adaptive process, shown in Fig. 7b, material efficiency decreases to 62.3% as the blade is distorted with increasing twist of -0.50 deg/mm. In comparison, the adaptive repair strategy, shown in Fig. 7c, maintains high material efficiency up to this level of twist in the out-of-service blade. From Table 1, it is also clear that chord length changes from nominal have a further deteriorating effect on material efficiency. This is particularly clear for non-adaptive repair of a twist of -0.26 deg/mm, where a chord length change of -0.125 - 0.02*z results in a 52.5% material efficiency, this compared to a 74.4% material efficiency for a similar repair involving no chord length change.

The process inefficiency associated with a non-adaptive repair strategy not only wastes raw material and processing time in the additive stage of a hybrid repair, but also increases processing time in the subsequent subtractive stage. To calculate weld deposition time, the total weld volume was divided by a conservative fine weld deposition rate, this taken to be that reported for Inconel 718 using a commercially available hybrid manufacturing machine [16]. The volume to be machined was calculated by performing the Boolean difference between the weld geometries and the blade geometries. This volume was then divided by a conventional material removal rate for Inconel 718 [17]. The resultant overall process time combining these two components of process time is shown in Fig. 8b. From the figure, significant savings can be achieved with an adaptive repair strategy as the actual blade geometry varies to a greater degree from the nominal geometry. In this regard, a non-adaptive hybrid repair framework could yield an approximately 94.1% increase in total processing time relative to an adaptive hybrid repair framework for a deformed blade with a twist of -0.5 deg/mm. Similarly, chord length changes would have a significant impact on the relative increases in overall processing time. This is particularly clear for non-adaptive repair of a twist of -0.26 deg/mm, where a chord length change of -0.125 - 0.02*z results in an increase in processing time of 102.4 seconds, this compared to an increase in processing time of 38.5 seconds for a similar repair involving no chord length change. Work is ongoing to further characterize the effects of adaptive repair strategies for more generalized part geometries.

5. Conclusion

A method of adaptive geometry transformation was developed for the re-manufacture of high valued components. The strategy was shown to be capable of accurately transforming nominal CAD geometry to

match that of a deformed sample geometry. Additional transformations were successfully performed on extended nominal geometry to re-create unknown geometry in a scenario common to hybrid part repairs in the aerospace sector. This overall strategy was shown to be successful in morphing a nominal part geometry to match that of a part to be machined with a maximum surface deviation of 0.011 mm. The resulting framework was implemented in an adaptive repair framework to determine additive weld placement. These experiments showed significant increases in material efficiency and decreases in hybrid repair processing time, these being sensitive to the degree of deformation (e.g., twist, chord length change) in the out-of-service part geometries. Future work will pursue further qualification of the of the algorithm, as well as deeper investigation into its effect on process efficiency.

Acknowledgements

This work was partially supported by Delta Airlines and NSF grants IIP-1631803 and CMMI-1646013.

References

[1] M. K. Thompson *et al.*, "Design for Additive Manufacturing: Trends, opportunities, considerations, and constraints," *CIRP Annals-Manufacturing Technology,* vol. 65, no. 2, pp. 737-760, 2016.

[2] J. B. Jones, P. McNutt, R. Tosi, C. Perry, and D. I. Wimpenny, "Remanufacture of turbine blades by laser cladding, machining and in-process scanning in a single machine," 2012.

[3] L. Ren, A. P. Padathu, J. Ruan, T. Sparks, and F. W. Liou, "Three dimensional die repair using a hybrid manufacturing system," *Austin, TX,* 2008.

[4] K. Karunakaran, S. Suryakumar, V. Pushpa, and S. Akula, "Retrofitment of a CNC machine for hybrid layered manufacturing," *The International Journal of Advanced Manufacturing Technology,* vol. 45, no. 7, pp. 690-703, 2009.

[5] S. Simhambhatla and K. Karunakaran, "Build strategies for rapid manufacturing of components of varying complexity," *Rapid Prototyping Journal,* vol. 21, no. 3, pp. 340-350, 2015.

[6] J. M. Flynn, A. Shokrani, S. T. Newman, and V. Dhokia, "Hybrid additive and subtractive machine tools–Research and industrial developments," *International Journal of Machine Tools and Manufacture,* vol. 101, pp. 79-101, 2016.

[7] H. Qi, M. Azer, and P. Singh, "Adaptive toolpath deposition method for laser net shape manufacturing and repair of turbine compressor airfoils," *The International Journal of Advanced Manufacturing Technology,* vol. 48, no. 1, pp. 121-131, 2010.

[8] P. Singh, H. Qi, M. N. Azer, and P. M. Kulkarni, "Laser net shape manufacturing and repair using a medial axis toolpath deposition method," ed: Google Patents, 2007.

[9] J. Zheng, Z. Li, and X. Chen, "Worn area modeling for automating the repair of turbine blades," *The International Journal of Advanced Manufacturing Technology,* vol. 29, no. 9, pp. 1062-1067, 2006.

[10] Y. Rong, J. Xu, and Y. Sun, "A surface reconstruction strategy based on deformable template for repairing damaged turbine blades," *Proceedings of the Institution of Mechanical Engineers, Part G: Journal of Aerospace Engineering,* vol. 228, no. 12, pp. 2358-2370, 2014.

[11] Z. Yun, C. Zhi-Tong, and N. Tao, "Reverse modeling strategy of aero-engine blade based on design intent," *The International Journal of Advanced Manufacturing Technology,* vol. 81, no. 9-12, pp. 1781-1796, 2015.

[12] Y. Dong, D. Zhang, K. Bu, Y. Dou, and W. Wang, "Geometric parameter-based optimization of the die profile for the investment casting of aerofoil-shaped turbine blades," *The International Journal of Advanced Manufacturing Technology,* vol. 57, no. 9-12, p. 1245, 2011.

[13] *GOM Inspect*. Available: http://www.gom.com/3d-software/gom-inspect.html

[14] P. J. Besl and N. D. McKay, "A method for registration of 3-D shapes," *IEEE Transactions on pattern analysis and machine intelligence,* vol. 14, no. 2, pp. 239-256, 1992.

[15] G. G. Slabaugh, "Computing Euler angles from a rotation matrix," *Retrieved on August,* vol. 6, no. 2000, pp. 39-63, 1999.

[16] T. Yamazaki, "Development of a hybrid multi-tasking machine tool: integration of additive manufacturing technology with CNC machining," *Procedia CIRP,* vol. 42, pp. 81-86, 2016.

[17] A. Sharman, R. C. Dewes, and D. K. Aspinwall, "Tool life when high speed ball nose end milling Inconel 718™," *Journal of Materials Processing Technology,* vol. 118, no. 1, pp. 29-35, 2001.